PNAS RESEARCH ARTICLE | NEUROSCIENCE

ISL1 is necessary for auditory neuron development and contributes toward tonotopic organization

Iva Filova[a,1], Kateryna Pysanenko[b,1], Mitra Tavakoli[a], Simona Vochyanova[a], Martina Dvorakova[a], Romana Bohuslavova[a], Ondrej Smolik[a], Valeria Fabriciova[a], Petra Hrabalova[a], Sarka Benesova[c], Lukas Valihrach[c], Jiri Cerny[d], Ebenezer N. Yamoah[e], Josef Syka[b], Bernd Fritzsch[f,g,2], and Gabriela Pavlinkova[a,2]

Edited by Christine Petit, Institut Pasteur, Paris, France; received May 1, 2022; accepted August 4, 2022

A cardinal feature of the auditory pathway is frequency selectivity, represented in a tonotopic map from the cochlea to the cortex. The molecular determinants of the auditory frequency map are unknown. Here, we discovered that the transcription factor ISL1 regulates the molecular and cellular features of auditory neurons, including the formation of the spiral ganglion and peripheral and central processes that shape the tonotopic representation of the auditory map. We selectively knocked out *Isl1* in auditory neurons using *Neurod1*^{Cre} strategies. In the absence of *Isl1*, spiral ganglion neurons migrate into the central cochlea and beyond, and the cochlear wiring is profoundly reduced and disrupted. The central axons of *Isl1* mutants lose their topographic projections and segregation at the cochlear nucleus. Transcriptome analysis of spiral ganglion neurons shows that *Isl1* regulates neurogenesis, axonogenesis, migration, neurotransmission-related machinery, and synaptic communication patterns. We show that peripheral disorganization in the cochlea affects the physiological properties of hearing in the midbrain and auditory behavior. Surprisingly, auditory processing features are preserved despite the significant hearing impairment, revealing central auditory pathway resilience and plasticity in *Isl1* mutant mice. Mutant mice have a reduced acoustic startle reflex, altered prepulse inhibition, and characteristics of compensatory neural hyperactivity centrally. Our findings show that ISL1 is one of the obligatory factors required to sculpt auditory structural and functional tonotopic maps. Still, upon *Isl1* deletion, the ensuing central plasticity of the auditory pathway does not suffice to overcome developmentally induced peripheral dysfunction of the cochlea.

spiral ganglion neurons | auditory nuclei | inferior colliculus | auditory maps | auditory behavior

Significance

Little is known about the molecular determinants of the auditory frequency maps. Our data provide insights into the functional role of the transcription factor ISL1 in the development of auditory neurons and in the formation of the auditory map. In this study, we found that selective genetic deletion of *Isl1* by *Neurod1*^{Cre} resulted in altered molecular and cellular characteristics of auditory neurons, affecting their migration, pathfinding abilities, and formation of peripheral and central processes. This neuronal phenotype was accompanied by hearing impairment, abnormalities in sound processing in the brain, and aberrant auditory behavior. These findings suggest that ISL1 is essential in regulating neuronal differentiation to produce functional auditory neurons.

Spiral ganglion neurons (SGNs) are bipolar, extending peripheral processes to the hair cells within the sensory epithelium (the organ of Corti) and central axons toward the cochlear nucleus (CN) complex, the first auditory nuclei in the brain. Sound-induced vibrations that reach the cochlea are amplified by the outer hair cells (OHCs) organized in three rows and innervated by type II SGNs. The inner hair cells (IHCs) receive, transduce, and transmit the auditory signal to type I SGNs that convey the signal via the vestibulocochlear cranial nerve to the CN of the brainstem. The auditory neurons are organized within the cochlea in an orderly fashion according to frequency, with high frequencies at the base and low frequencies at the apex (1, 2). The tonotopic organization of type I SGNs corresponds to multiple diversities in their molecular profiles, connectivity patterns, and physiological features along the tonotopic axis (3–6). The cochleotopic or tonotopic pattern is maintained throughout the auditory pathways in the brain (7). The central auditory pathway transmits ascending acoustic information from the CN through the lateral lemniscus complex, the inferior colliculus (IC) in the midbrain, and the medial geniculate nucleus of the thalamus to the auditory cortex (8). The efferent motor neurons consist of the medial olivocochlear motor neurons, which modulate cochlear sound amplification by OHCs. In contrast, lateral olivocochlear motor neurons innervate afferent type I sensory neurons and regulate cochlear nerve excitability (8–10).

The cellular and molecular regulation of neuronal migration and the establishment of tonotopic connections to the hair cells or neurons of the hindbrain's first auditory nuclei, the CN, are not fully understood. Several transcription factors govern the development of inner ear neurons, including NEUROG1 (11), NEUROD1 (12), GATA3 (13, 14), and POU4F1 (15). The transcription factor NEUROD1 is vital for the differentiation and survival of inner ear neurons (16–18). We previously demonstrated that *Isl1*^{Cre}-mediated *Neurod1* deletion (*Neurod1CKO*) results in a disorganized cochleotopic projection from SGNs (19), affecting acoustic information processing in the central auditory system of adult mice at the physiological and behavioral levels (20). During inner ear development, ISL1 is expressed in the differentiating neurons and sensory precursors (19, 21, 22). *Isl1* is

Author contributions: J.S., B.F., and G.P. designed research; I.F., K.P., M.T., S.V., M.D., R.B., V.F., P.H., and B.F. performed research; I.F., K.P., M.T., S.V., M.D., R.B., O.S., V.F., S.B., L.V., J.C., J.S., B.F., and G.P. analyzed data; and E.N.Y., J.S., B.F., and G.P. wrote the paper.

The authors declare no competing interest.

This article is a PNAS Direct Submission.

[1]I.F. and K.P. contributed equally to this work.

[2]To whom correspondence may be addressed. Email: bernd-fritzsch@uiowa.edu or Gabriela.Pavlinkova@ibt.cas.cz.

This article contains supporting information online at http://www.pnas.org/lookup/suppl/doi:10.1073/pnas.2207433119/-/DCSupplemental.

Published September 8, 2022.

expressed in all four populations of SGNs (type Ia, Ib, Ic, and type II) identified by single-cell RNA sequencing (4). Studies suggest that ISL1 plays a role in developing neurons and sensory cells, but there has been no direct evaluation of ISL1 function in the inner ear. Using *Neurod1*^{Cre} (23), we conditionally deleted *Isl1* (*Isl1CKO*) in neurons without directly affecting the development of the inner ear sensory epithelium.

This work provides genetic and functional evidence for ISL1's role in establishing the spiral ganglion peripheral projection map and proper central auditory circuitry. Most *Isl1CKO* neurons migrated into the center of the cochlear modiolus, in contrast to control animals, with an arrangement of SGNs in parallel to the spiraling cochlear duct. Additionally, we analyzed the transcriptome of neurons, hearing function, sound information processing in the IC, and auditory behavior of *Isl1CKO* to demonstrate how abnormal SGN development affects the formation, wiring, and operation of the auditory sensory maps.

Results

ISL1 Controls Neuronal Phenotype in the Cochlea. To investigate the role of ISL1 in inner ear neuron development, we eliminated *Isl1* by crossing *Isl1*$^{loxP/loxP}$ mice (24) with *Neurod1*^{Cre} mice (23). *Neurod1*^{Cre} is expressed in sensory neurons but not in the sensory epithelium (*SI Appendix*, Fig. S1). Analyses of ISL1 expression in *Isl1CKO* confirmed efficient recombination by *Neurod1*^{Cre} with virtually no expression of ISL1 during the differentiation of neurons in the inner ear ganglion as early as embryonic day (E)10.5, and later in the cochlear neurons, shown at E14.5 and postnatal day 0 (P0), in contrast to high levels of ISL1 in neurons in the control inner ear (*SI Appendix*, Fig. S2). It is worth mentioning that no difference was observed in the density of Schwann cells (*SI Appendix*, Fig. S2 *E* and *F*).

The organization of the sensory epithelium in the organ of Corti of *Isl1CKO* was comparable to controls in the basal but not the apical part, with three rows of OHCs and one row of IHCs (Fig. 1 *A*–*F*). Whole-mount antitubulin staining of innervation showed reduced and disorganized radial fibers with large gaps between radial fiber bundles, crisscrossing fibers, and an unusual dense innervation in the apex, with some large fiber bundles bypassing the organ of Corti and extending to the lateral wall in the *Isl1CKO* cochlea (arrowhead in Fig. 1*F*).

Next, we evaluated the effects of *Isl1* deletion on the formation of the spiral ganglion. The SGN somas were well restricted to the Rosenthal's canal in control animals, arranged in a spiral parallel to the cochlear duct (Fig. 1 *G*–*I*). In contrast, unevenly distributed neurons were found in *Isl1CKO* with many SGNs accumulated beyond the Rosenthal's canal, in the conical central part of the cochlea, the modiolus (Fig. 1 *J*–*L*), which usually carries only afferent and efferent fibers. The unusual accumulation of cochlear

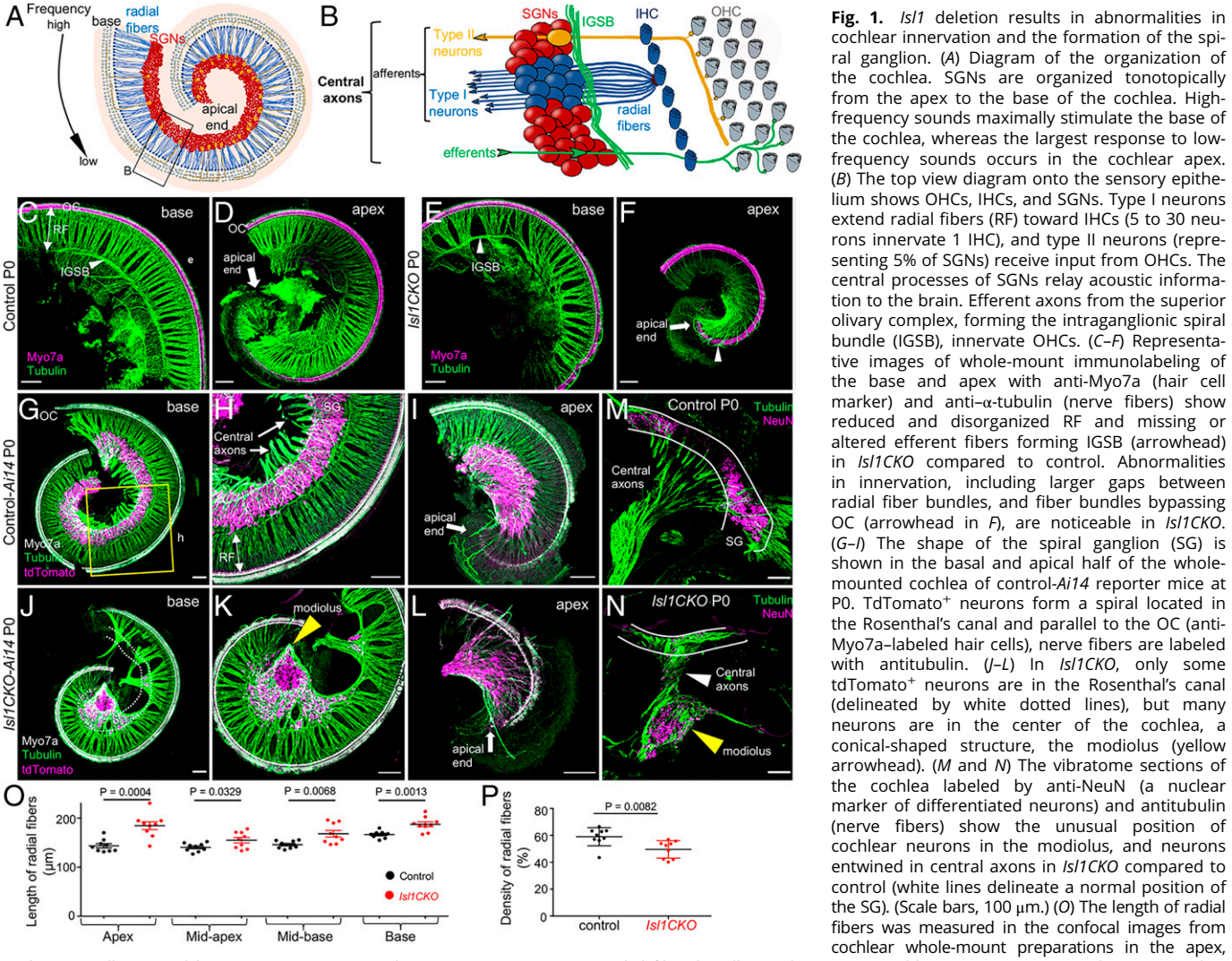

Fig. 1. *Isl1* deletion results in abnormalities in cochlear innervation and the formation of the spiral ganglion. (*A*) Diagram of the organization of the cochlea. SGNs are organized tonotopically from the apex to the base of the cochlea. High-frequency sounds maximally stimulate the base of the cochlea, whereas the largest response to low-frequency sounds occurs in the cochlear apex. (*B*) The top view diagram onto the sensory epithelium shows OHCs, IHCs, and SGNs. Type I neurons extend radial fibers (RF) toward IHCs (5 to 30 neurons innervate 1 IHC), and type II neurons (representing 5% of SGNs) receive input from OHCs. The central processes of SGNs relay acoustic information to the brain. Efferent axons from the superior olivary complex, forming the intraganglionic spiral bundle (IGSB), innervate OHCs. (*C*–*F*) Representative images of whole-mount immunolabeling of the base and apex with anti-Myo7a (hair cell marker) and anti–α-tubulin (nerve fibers) show reduced and disorganized RF and missing or altered efferent fibers forming IGSB (arrowhead) in *Isl1CKO* compared to control. Abnormalities in innervation, including larger gaps between radial fiber bundles, and fiber bundles bypassing OC (arrowhead in *F*), are noticeable in *Isl1CKO*. (*G*–*I*) The shape of the spiral ganglion (SG) is shown in the basal and apical half of the whole-mounted cochlea of control-*Ai14* reporter mice at P0. TdTomato^{+} neurons form a spiral located in the Rosenthal's canal and parallel to the OC (anti-Myo7a–labeled hair cells), nerve fibers are labeled with antitubulin. (*J*–*L*) In *Isl1CKO*, only some tdTomato^{+} neurons are in the Rosenthal's canal (delineated by white dotted lines), but many neurons are in the center of the cochlea, a conical-shaped structure, the modiolus (yellow arrowhead). (*M* and *N*) The vibratome sections of the cochlea labeled by anti-NeuN (a nuclear marker of differentiated neurons) and antitubulin (nerve fibers) show the unusual position of cochlear neurons in the modiolus, and neurons entwined in central axons in *Isl1CKO* compared to control (white lines delineate a normal position of the SG). (Scale bars, 100 μm.) (*O*) The length of radial fibers was measured in the confocal images from cochlear whole-mount preparations in the apex, midapex, midbase, and base. Data are expressed as mean ± SEM (n = 3 radial fiber bundles/each region/3 cochlea/genotype); unpaired t-test. (*P*) Fiber density was quantified in the base, midbase, and midapex (n = 3 mice per genotype). Error bars represent mean ± SD; unpaired t-test.

neurons intertwined with the central axons in the modiolus of *Isl1CKO* is depicted in the cochlear sections (Fig. 1 *M* and *N*). In line with the unusual position of SGNs, the radial fibers were significantly lengthened in all regions of the *Isl1CKO* cochlea (Fig. 1*O*), but the overall radial fiber density was reduced (Fig. 1*P*). We performed immunostaining for cleaved Caspase-3 (*SI Appendix*, Fig. S3) to determine whether neuron number was affected by apoptosis during inner ear development. Most apoptotic neurons were found outside the cochlea in the vestibular ganglion (VG) area in E14.5 *Isl1CKO*, implying that missing neurons in the Rosenthal's canal are due to the altered migration of SGNs rather than neuronal death in the developing inner ear.

Interestingly, *Isl1* deficiency caused a shortening of the cochlea, which was on average ∼20% and 25% shorter at P0 and in adults, respectively (*SI Appendix*, Fig. S4 *A* and *B*). Since *Neurod1*^{Cre} is expressed only in neurons, the shortening of the cochlea appears to be a secondary effect of the abnormalities in neuronal development. A similar phenotype of truncated growth of the cochlea was reported for *Neurod1* and *Neurog1* mutants because of alternations in spatiotemporal gene expression (11, 19, 20, 25). Correspondingly to the truncated cochlear phenotype (11, 19, 20, 25), detailed analyses showed abnormalities in the epithelium at the apical end with disorganized rows of OHCs and ectopic IHCs among OHCs in the *Isl1CKO* cochlea (*SI Appendix*, Fig. S4*C*). The disorganized apical epithelium represented ∼11.8% of the length of the organ of Corti in adults. Antitubulin labeling revealed a reduced and disorganized innervation in the region of OHCs in *Isl1CKO* (*SI Appendix*, Fig. S4*D*). In the controls, fibers extending through the tunnel of Corti were oriented toward the base to form three parallel outer spiral bundles. In contrast, guiding defects in the extension of these fibers in *Isl1CKO* were apparent, with neurites extending with random turns toward the base and the apex (arrowheads in *SI Appendix*, Fig. S4*D*). To further investigate cochlear histopathology in *Isl1CKO*, we evaluated synaptic contacts from type I SGNs onto IHCs in 2-mo-old mice (*SI Appendix*, Fig. S4*E*). CtBP2^{+} ribbon synapse number was reduced in *Isl1CKO*, representing ∼46%, 51%, 56%, and 69% ribbons of the control base, midbase, midapex, and apex, respectively (*SI Appendix*, Fig. S4*F* and Table S1). Altogether, these results demonstrate the prominent effects of *Isl1* deletion on the formation of the spiral ganglion and innervation patterns in the cochlea.

ISL1 Regulates Neuronal Identity and Differentiation Programs of SGNs. To gain insight at the molecular level on how the *Isl1* elimination causes the neuronal phenotype in the cochlea, we sought to identify potential ISL1 targets through global transcriptome analysis. We opted to use Bulk-RNA sequencing to obtain sequencing depth and high-quality data (25). Six biological replicates were used per genotype, and each replicate contained a total of 100 tdTomato^{+} SGNs isolated from the E14.5 cochlea (Fig. 2*A*). By E14.5, sensory neurons cease to proliferate and are undergoing active differentiation and axonogenesis. Compared to controls, 650 protein-coding genes were differentially expressed in *Isl1CKO* neurons (Fig. 2*B* and Dataset S1). Gene ontology (GO) term enrichment analysis revealed highly enriched GO terms associated with neuron development, including "neurogenesis," "neuron differentiation," and "nervous system development" (Fig. 2*C* and Dataset S2). The most enriched and specific GO categories for down-regulated genes were associated with neurotransmission-related machineries, such as "transmembrane transporter," "voltage-gated channel," "cation and ion transport," and "membrane potential regulation," indicating changes in neuronal cell functions. The analysis identified enrichment of down-regulated genes involved in axon development, guidance, axonogenesis, and neuronal migration, including members of all four axon guidance molecules and their cognate receptors, the ephrins-Eph, semaphorins-plexin, netrin-unc5, and slit-roundabout (27). The neurotrophic tyrosine kinase receptors (*Ntrk2* and *Ntrk3*) and a G protein-coupled chemokine receptor (*Cxcr4*), important regulators of neuronal migration, were also down-regulated (28).

In contrast, up-regulated genes particularly enriched in *Isl1CKO* neurons were associated with "regulation of synapse organization,

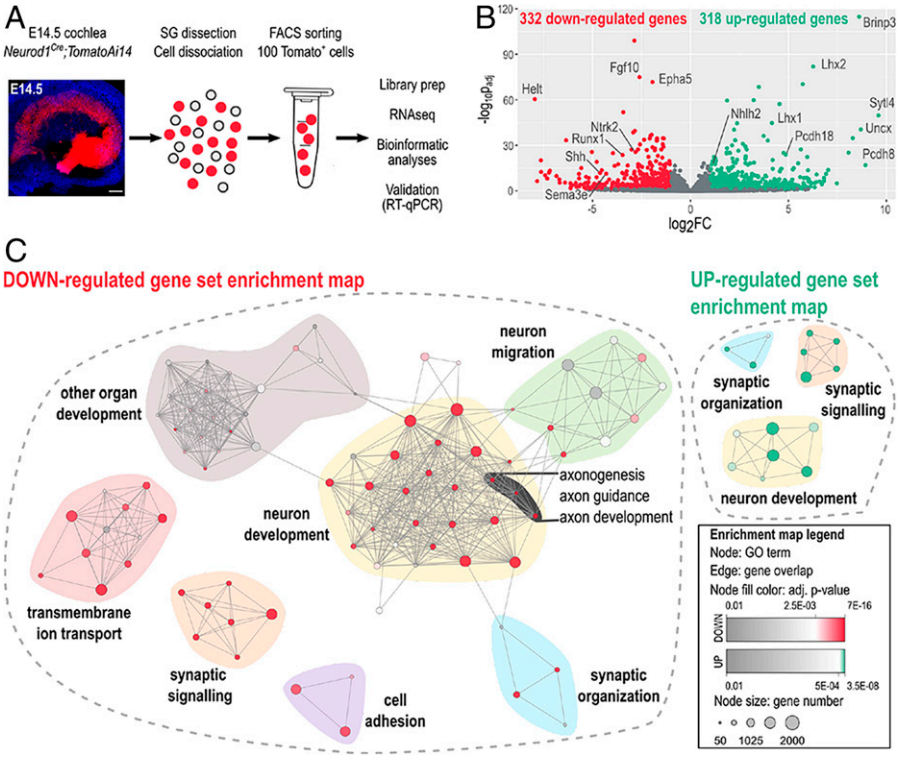

Fig. 2. ISL1-mediated transcription signature in cochlear neurons. (*A*) Image of the whole-mount cochlea with genetically labeled tdTomato neurons in the spiral ganglion at E14.5 (Hoechst staining, blue). (Scale bar, 100 μm.) Workflow depicts microdissection, dissociation, FACS sorting of single tdTomato^{+} SGNs for a bulk of 100 cells RNA-sequencing (RNAseq) analysis. (*B*) The volcano plot shows the change in protein-coding gene expression levels in the *Isl1CKO* compared to control spiral ganglion neurons (adjusted $P < 0.05$, and fold-change > 2 cutoff values). The complete list of identified 332 down- and 318 up-differentially expressed genes is in Dataset S1. (*C*) Enrichment map of down- and up-regulated GO sets visualized by the network. Each node represents a GO term; edges depict shared genes between nodes. Node size represents a number of genes of the mouse genome per the GO term, and node fill color represents a GO term significance. Each GO set cluster was assigned with representative keywords; a list of GO sets is available in Dataset S2.

synapse structure or activity" and "regulation of synapse assembly," indicating changes relating to the ability of neurons to form neuronal projections toward their targets. Up-regulated genes encoding molecules critical for synapse formation and adhesion included several members of the cadherin superfamily (*Cdh7*, *Cdh10*, *Pcdh8*, *Pcdh9*, *Pcdh10*, *Pcdh18*, and *Pcdh19*), adhesion-related genes (*Ptprd*, *Ptprs*, *Cntnap2*, *Itga4*, and *Itga5*), and the ephrin ligands (*Efna3* and *Efna5*). Interestingly, "synaptic signaling" was among GO terms with significant representation in both up- and down-regulated genes, suggesting changes in synaptic circuits and neuronal activity. We also found many genes encoding transcription factors and signaling molecules, indicating that ISL1 may act through transcription networks instead of defined target genes. The expression of neural-specific basic helix-loop-helix (bHLH) factors important for differentiation and maturation of neurons was increased in *Isl1CKO*, including members of NeuroD (*Neurod6* and *Neurod2*), Nscl (*Nhlh2*), and Olig (*Bhlhe23*) families (29). Genes encoding LIM domain proteins, the transcription factors *Lhx1*, *Lhx2*, *Lmo2*, and *Lmo3*, a core member of the PCP signaling paradigm, *Prickle1*, and neuronal homeobox genes, *Emx2*, *Uncx*, and *Pknox2* were up-regulated in *Isl1CKO* neurons. *Prickle1* is an essential regulator of neuron migration and neurons' distal and central projections in the cochlea (30). Some of the identified genes encoding regulatory molecules shown to be essential for neuronal development, the formation of SGNs, and their projections were down-regulated in *ISL1CKO* neurons, such as the signaling molecules *Shh* (31), *Wnt3* (3), and *Fgfs* (*Fgf10*, *Fgf11*, and *Fgf13*) (32, 33), and the transcription factors *Gata3* (13, 14), *Irx1*, *Irx2*, *Pou3f2*, *Pou4f2*, and *Runx1* (3, 4).

Consistent with the idea that ISL1 may control a gene-expression program mediating different aspects of neuronal development in the cochlea, several identified genes are known to affect the formation of SGNs and their innervation patterns. For example, a mouse model with EphA4-deficient signaling in SGNs results in aberrant mistargeting of type I projections to OHCs (34) and SGN fasciculation defects (35). Targeted disruptions of the neurotrophin receptors, *Ntrk2* and *Ntrk3*, are associated with misplaced SGNs in the modiolus, disorganized projections, and reduced neuronal survival (36). The neurotrophin receptor p75NTR (*Ngfr*)-deficient SGNs demonstrate enhanced neurite growth behavior (37). Mutation of *Prickle1* results in disorganized apical afferents (30). Reduced and aberrant cochlear innervation was shown in mice with *Gata3*-specific SGN deletion (14). *Nrp2* expressed in SGNs is required for axon path finding and a normal pattern of cochlear innervation (38). The axon guidance molecule SLIT2 and its receptor ROBO1/2 control precise innervation patterns, and their deletions induce misplacement of SGNs (39). Mice lacking *Dcc* have the more severe phenotype of mislocated SGNs and disorganized central projections, although most SGNs of $Dcc^{-/-}$ remained within Rosenthal's canal (40). These molecular differences dovetail well with abnormalities in the innervation pattern and SGN migration defects *Isl1CKO*. *Dcc*, *Epha5*, *Ntng1*, *Prdm8*, *Robo2*, *Slit2*, *Tbx3*, *Uncx*, *Gata3*, *Lhx1*, *Lhx2*, *Cdh7*, *Nhlh2*, *Ntrk2*, and *Ntrk3* were further validated by qRT-PCR of RNA isolated from whole inner ears of E14.5 embryos (*SI Appendix*, Fig. S5). These changes indicate that ISL1 regulates transcriptional networks that underlie neuronal identity and function during differentiation of SGNs and that *Isl1* elimination results in a major impairment in the development, axonogenesis, migration, and molecular characteristics of these neurons.

***Isl1CKO* Mice Have Altered Hearing Function.** Considering the substantial abnormalities in the formation of the spiral ganglion, innervation, and molecular neuron features, we assessed the hearing function of *Isl1CKO*. We evaluated distortion product otoacoustic emissions (DPOAE) to determine the robustness of OHC function and cochlear amplification. Compared to controls, the DPOAE responses of *Isl1CKO* were significantly reduced in the frequency range between 4 and 24 kHz (Fig. 3*A*). DPOAE amplitudes at frequencies of 26 kHz and higher were comparable between control and *Isl1CKO* mice. Based on the physiological place-frequency map in the normal mouse cochlea (41), frequencies above 26 kHz are located at the basal half of the cochlea. Thus, decreased DPOAE responses may be attributed to the more profound morphological abnormalities in the apex, disorganized innervation, and disorganized rows of OHCs in the apical end.

We evaluated auditory brainstem responses (ABRs), which measure electrical activity associated with the propagation of acoustic information through auditory nerve fibers. Measurements of ABR thresholds showed that all *Isl1CKO* animals displayed elevated thresholds indicative of hearing loss compared

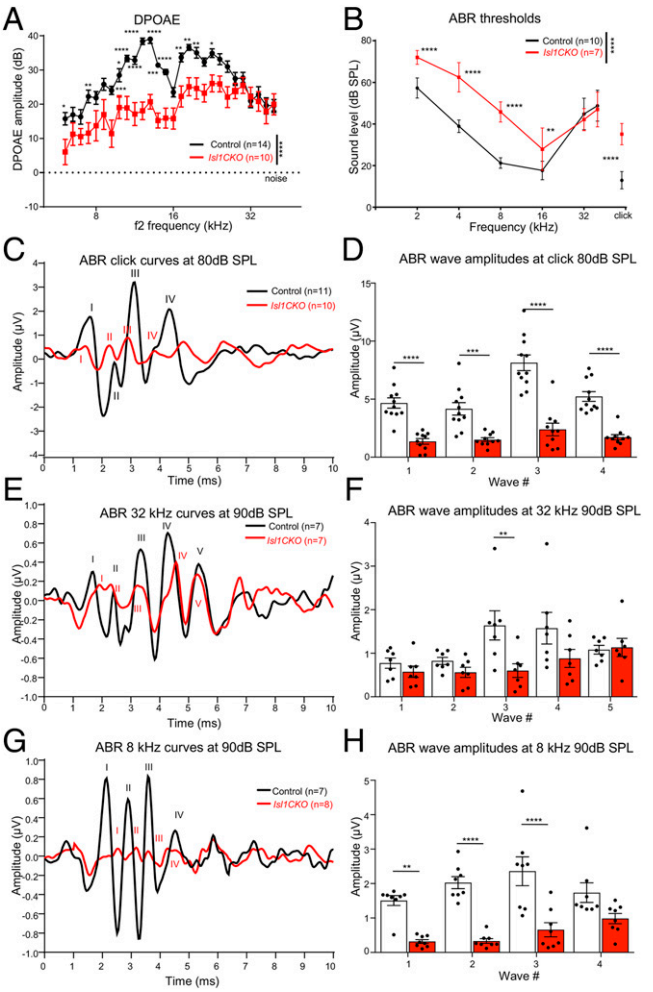

Fig. 3. Hearing impairment is detected in *Isl1CKO* mice. (*A*) DPOAEs show significantly reduced levels in the low and middle-frequency range (4 to 24 kHz), stimuli intensities L1/L2 = 70/60-dB SPL. Data are expressed as mean ± SEM. (*B*) The average ABR thresholds of *Isl1CKO* and control mice are analyzed by click-evoked ABR. Data are expressed as mean ± SD. (*C*) Averaged ABR response curves evoked by an 80-dB SPL click; (*E*) by a 90-dB SPL pure tone of 32-kHz frequency; and (*G*) by a 90-dB SPL pure tone of 8-kHz frequency are presented. (*D*, *F*, and *H*) Averaged individual ABR wave amplitudes are shown for the corresponding peaks. Data are expressed as mean ± SEM. Two-way ANOVA with Bonferroni post hoc tests $*P < 0.05$, $**P < 0.01$, $***P < 0.001$, $****P < 0.0001$.

to age-matched control animals, except at frequencies 32 and 40 kHz, which were comparable to ABR thresholds in control mice (Fig. 3*B*). Using click-evoked ABR, we evaluated waveform characteristics associated with the propagation of acoustic information through the auditory nerve to higher auditory centers (Fig. 3*C*). Wave I reflects the synchronous firing of the auditory nerve. In contrast, waves II to V are attributed to the electrical activity of downstream circuits in the CN, superior olivary complex, lateral lemniscus, and IC (42). Waves IV and V are products of the sound-evoked neuronal activity in the lateral lemniscus and IC (43–45). The waves IV and V are often paired and superimposed in commonly used nontransgenic mouse strains (44, 45). The ABR traces in all of our panels were averaged traces from all measured animals. A part of the animals in both experimental groups had a hardly distinguishable wave V in response to the click and 8-kHz sound stimulation; therefore, to prevent bias, we did not include wave V. The amplitudes of ABR waves I to IV were significantly reduced in *Isl1CKO* (Fig. 3*D*). Since the ABR thresholds for 32 kHz and above were comparable between age-matched controls and *Isl1CKO* (Fig. 3*B*), we used the pure-tone stimuli of 32 kHz to evaluate ABR responses (Fig. 3*E*). A significant difference among the genotypes was found only for amplitude reduction of wave III (Fig. 3*F*), thus indicating preserved synchronized activities of peripheral and brainstem auditory processing. Although waves I and II amplitude for both mutant and control mice were similar, there were apparent differences in the ABR waveform morphology. The latency of ABR wave I was delayed, the relative interwave latency between peaks I and II was shortened, and the trough between wave I and II diminished, resulting in a fusion of both peaks in *Isl1CKO*. A delay of the leading peak of ABR wave I recovered toward ABR wave III. The wave I and II changes reflect abnormalities in the summated response from SGNs, auditory nerve fibers, and most likely the CN.

Additionally, we used a pure-tone stimulus of 8 kHz to evaluate ABR responses (Fig. 3*G*), as ABR thresholds for 8 kHz were significantly reduced for *Isl1CKO* mice. In contrast to ABR amplitudes at 32-kHz stimuli, ABR amplitudes for 8-kHz pure-tone stimuli were significantly reduced for I to III waves (Fig. 3*H*). The results indicate abnormalities in the cochlear auditory neurons and propagation of acoustic information through auditory nerve fibers to higher auditory centers. We observed a marked drop in the wave I growth function. Still, by comparing wave I and IV peaks, an increased central gain was noted in *Isl1CKO* (*SI Appendix*, Fig. S6), indicating neural plasticity at higher auditory circuits for cochlear damage with diminished afferent input (46).

***Isl1CKO* Mice Display Abnormalities in the Ascending Auditory Pathways.** Having recognized uneven hearing function loss, as measured by ABRs, we further wanted to investigate the distribution of SGNs in the *Isl1CKO* cochlea and the morphology of the components of the central auditory pathway. We generated three-dimensional (3D) visualization of the cochlea using light-sheet fluorescent microscopy (Fig. 4 *A*–*I* and Movies S1–S4). In the first cochlear preparation, neurons were visualized by *tdTomato* reporter expression and hair cells in the organ of Corti were labeled using anti-Myo7a. In the second preparation, tdTomato$^+$ neurons were colabeled with anti-NeuN, a nuclear marker of differentiated neurons. Compared to the recognizable coil of SGNs in the controls (Fig. 4 *A*–*C* and Movies S1 and S2), SGNs were aberrantly distributed in the *Isl1CKO* cochlea (Fig. 4 *D*–*I* and Movies S3 and S4). Many *Isl1CKO* neurons were in the center of the cochlea, the modiolus, that normally contains only central processes of SGNs, as shown in the control cochlea (Fig. 4 *B* and *C*). Some *Isl1CKO* neurons were found in their proper position in Rosenthal's canal, forming a dense strip of neurons, suggesting a partially preserved organization of the spiral ganglion (Fig. 4 *F* and *I*). This segment of the spiral ganglion formed in the midbase of the *Isl1CKO* cochlea correlates with the estimated characteristic place in the cochlear place-frequency map for the characteristic frequency (CF) of 32 kHz (40) (Fig. 4*J*). Partial preservation of the spiral ganglion in the midbase corresponds to the retained high-frequency hearing function of *Isl1CKO*. Identical to the SGN migration abnormalities recognized at P0, most SGNs were in the modiolus, outside of Rosenthal's canal, in *Isl1CKO* adult mice (*SI Appendix*, Fig. S7). Apart from the changes in the cochlear ganglion, the VG was fused and enlarged in *Isl1CKO* compared to distinct superior and inferior vestibular ganglia in controls (Fig. 4 *K* and *L*). The spatial segregation between the vestibular and spiral ganglion was diminished in *Isl1CKO*, with some areas fused, and thus, forming an aberrant "spiro-vestibular" ganglion.

Using dye tracing, we evaluated the segregation of central axons of the auditory nerve (the cranial nerve VIII) (Fig. 5*A*, schematic view of dye applications). In controls, the central axons labeled by dyes applied into the base and apex are segregated in the auditory nerve and from the VG, labeled by dye injected into the vestibular end-organs (Fig. 5*B*). In contrast, the central axons virtually overlapped in the auditory nerve (yellow fibers), and neurons labeled by cochlear dye applications were detected to be intermingled with vestibular neurons in an aberrant "spiro-vestibular" ganglion in *Isl1CKO* (Fig. 5*C*). Unfortunately, the mixing of spiral and VG neurons in *Isl1CKO* mice precluded a full quantitative assessment.

The CN is the first structure of the ascending auditory pathways, where the auditory nerve fibers project. The auditory nerve bifurcated with one branch, synapsing in the posteroventral and dorsal CN (DCN) and the other innervating the anteroventral CN (Fig. 5*A*). Dye tracing showed segregated projections of apical and basal cochlear afferents forming parallel isofrequency bands in controls at E16.5 (Fig. 5*D*). In contrast, comparable injections in *Isl1CKO* showed that axonal projections to the CN were reduced, restricted, disorganized, and lacked clear apex- and base-projection segregations, as many fibers overlapped (Fig. 5 *E*–*G*). Only a few fibers can occasionally be seen expanding to the DCN in *Isl1CKO* at E16.5 (*Inset* in Fig. 5*E*). Aberrant central projections were further demonstrated by cochlear neurons projecting to the lateral vestibular nucleus in *Isl1CKO* (Fig. 5*I*). No such projections were found in control mice with segregated vestibular projections to the vestibular nucleus, and basal and apical afferents reaching the CN (Fig. 5*H*). Collectively, these data show disorganized central projections and a loss of tonotopic organization of both the auditory nerve and the CN in *Isl1CKO*, as the apical and basal projections are not completely segregated (see graphic summary in Fig. 5*J*).

Since the size and number of neurons in the CN depend on input from the auditory nerve during a critical development period (47), we analyzed the volume of the CN of *Isl1CKO*. The volume of the CN of mutants was reduced by ∼50% compared to controls at P35 (*SI Appendix*, Fig. S8). As *Isl1* is not expressed in the CN (20), the reduced size is likely a secondary effect associated with reduced afferent input consistent with the previously reported impact of neonatal cochlear ablation (2). The spherical and globular bushy cells are principal cells that receive large auditory nerve endings, called "endbulbs of Held" and "modified endbulbs," specialized for precise temporal firing (1, 48). Using

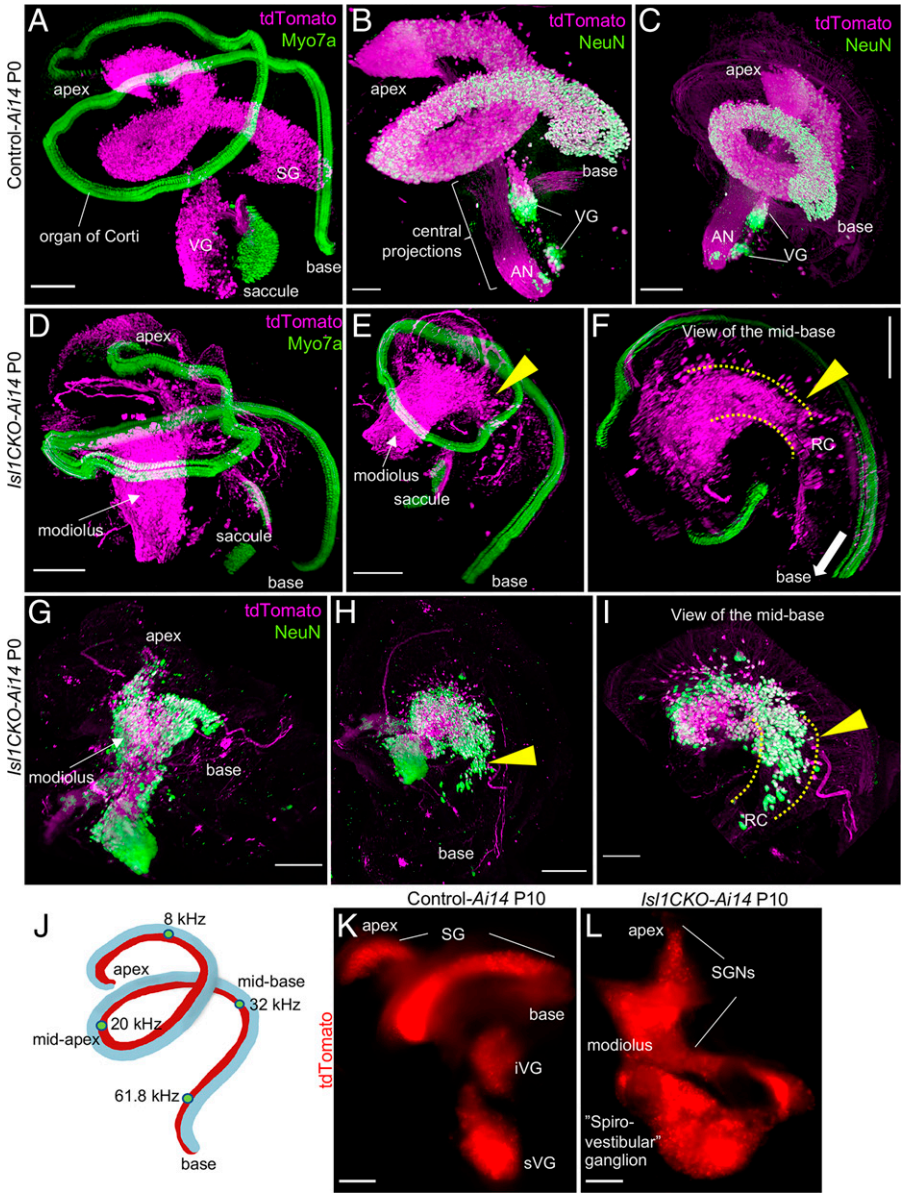

Fig. 4. Neurons in the *Isl1CKO* inner ear are abnormally distributed. (*A–I*) Microdissected cochleae of reporter control-*Ai14* and *Isl1CKO-Ai14* mice were cleared (CUBIC protocol), immunolabeled, imaged, and reconstructed in 3D using light-sheet fluorescence microscopy (Movies S1–S4). (*A*) In the control cochlea, tdTomato$^+$ SGNs form a coil of the SG in the Rosenthal's canal and anti-Myo7a–labeled hair cells show the spiral shape of the organ of Corti. Parts of the VG with tdTomato$^+$ neurons and the saccule with Myo7a$^+$ hair cells are shown. (*B* and *C*) Anti-NeuN (a nuclear marker of differentiated neurons) colabeled tdTomato$^+$ neurons form the SG and VG in the control cochlea; the modiolus contains the central processes, forming the auditory nerve (AN). (*D–F*) In *Isl1CKO-Ai14*, tdTomato$^+$ neurons are mainly located in the conical central part of the cochlea, the modiolus, in contrast to the spiral of the organ of Corti with Myo7a$^+$ hair cells. Some *Isl1CKO* neurons form a segment of the SG in the Rosenthal's canal (RC) in the midbase region (arrowhead), shown in detail in *F*; the RC area is highlighted by dotted lines. (*G* and *H*) Abnormal and uneven distribution of cochlear tdTomato$^+$ neurons is shown by anti-NeuN colabeling. Many neurons are misplaced in the modiolus, but some neurons are in their close-normal position in the Rosenthal's canal (arrowhead). (*J*) Schematic drawing of the mouse cochlea shows the cochlear place-frequency map for four cochlear regions termed the apex (corresponding to the best encoding frequencies ~8 kHz at the distance from the basal end of 82%), midapex (~19 kHz at 49% length), midbase (~32 kHz at 32% length), and basal turn (~62 kHz at 9% length) (41). (*K*) Whole-mount images of the P10 inner ear show distribution of tdTomato-labeled neurons in superior (sVG) and inferior VG (iVG), and SG in the control-*Ai14*. (*L*) In the *Isl1CKO-Ai14*, the VG is fused and enlarged, spatial segregation between the VG and SG is diminished, forming an aberrant "spiro-vestibular" ganglion, and the SG has lost its spiral shape. (Scale bars: 200 μm in all panels, except for *B* and *I*, which are 100 μm.)

antiparvalbumin to label spherical bushy cells and anti-VGlut1 to label auditory nerve endbulbs of Held (49, 50), we demonstrated that auditory afferents of *Isl1CKO* and controls formed comparable clusters of boutons that wrap the somas of their targets and the density of bushy cells was similar (*SI Appendix*, Fig. S8 *C–H*).

Characteristics of IC Neurons Are Distorted in *Isl1CKO*. We evaluated IC properties, which is the principal auditory structure of the midbrain for the ascending auditory pathways and descending inputs from the auditory cortex (51). The IC allows for sound localization, integrates multisensory and nonauditory contributions to hearing, and plays an essential role in generating the startle response. We demonstrated no significant IC size reduction in *Isl1CKO* compared to controls (Fig. 6 *A* and *B*). We compared neuronal characteristics in the central nucleus of the IC of *Isl1CKO* and control animals using multichannel electrodes. Compared to a well-defined narrow single-peaked profile of the excitatory receptive field in controls, we recorded the multipeaked broad tuning curves in the IC of *Isl1CKO*, suggesting multiple inputs from the lower levels of the auditory system and the worsened tunning characteristics of IC neurons (Fig. 6*C*).

The investigation of the responsiveness of IC neurons (IC units) to different sound frequencies showed higher excitatory thresholds in *Isl1CKO* compared to controls in measured frequencies between 6 and 28 kHz (Fig. 6 *D* and *E*). Responsiveness of IC units to recorded frequencies above 28 kHz was comparable between control and mutant mice. These comparable thresholds for high frequencies between control and *Isl1CKO* mice are consistent with the ABR measurements. At the low-frequency range, below 6 kHz, we did not record any IC neurons in *Isl1CKO*. Compared to the controls, the IC neuronal responses in *Isl1CKO* had a higher broadband noise (BBN) threshold, a narrower dynamic range, higher spontaneous activity, and a lower maximum response magnitude (Fig. 6*F*), suggesting a functional reduction in sensitivity to sound, audibility, intensity discrimination, and increased excitability of IC neurons in *Isl1CKO*. A commonly used metric unit of auditory tuning is the "quality factor" or Q, defined as the CF divided by the bandwidth, measured at 20 dB above the minimum threshold (Q_{20}). Results revealed a significantly lower

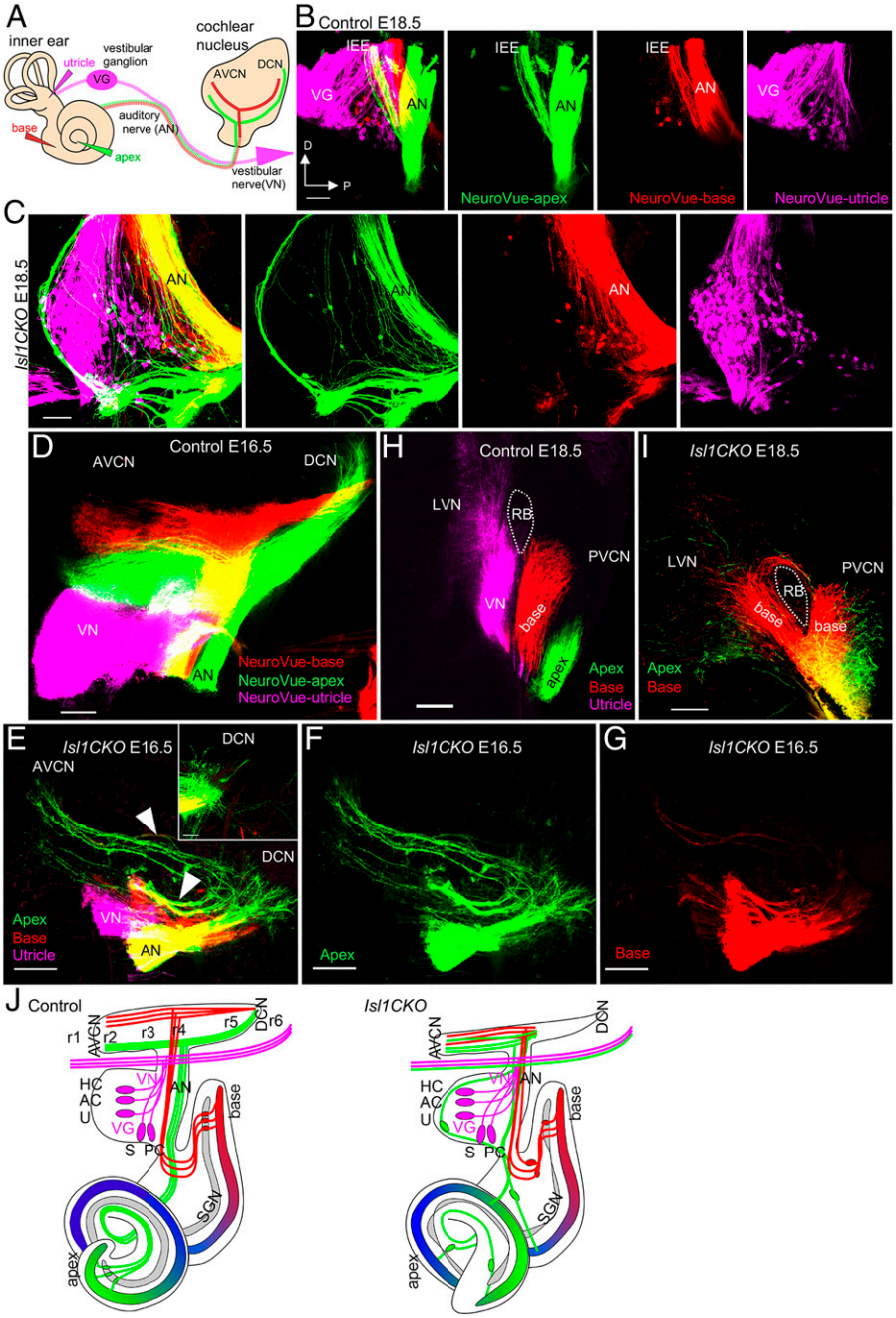

Fig. 5. *Isl1CKO* neurons project unsegregated and disorganized central projections to the CN. (*A*) The schematic diagram visualizes dye tracing from the inner ear and its connections to the auditory brainstem, using insertions of differently colored NeuroVue dyes into the vestibular end-organ (utricle, magenta), cochlear base (red), and apex (green). Axonal projections from cochlear neurons to the CN bifurcate with one branch synapsing in the DCN and the other innervating the anteroventral CN (AVCN). (*B*) Images of individual colors of the separate channels and a merged image show distinct and spatially restricted bundles of neuronal fibers of the auditory nerve (AN) projecting to the CN and the VG in controls, labeled by dye applications. The only mixed bundle (yellow) is inner ear efferents (IEE). (*C*) In *Isl1CKO*, the segregation of central axons is lost, as fibers labeled from the apex and base are mainly overlapping in the AN (yellow fibers), and neurons labeled by dyes applied into the cochlear base and apex are mixed with VG neurons to form an aberrant ganglion, the "spiro-vestibular" ganglion. Note that fibers labeled from the apex (green) form an unusual fiber loop around the ganglion, and no IEE are recognizable in *Isl1CKO*. (*D*) The tonotopic organization of the CN subdivisions is shown with low-frequency afferents labeled from the apex (green) and high frequency from the base (red) and organized as parallel fibers in isofrequency bands in controls at E16.5. (*E*) In *Isl1CKO*, cochlear afferents enter the AVCN as a single bundle instead of forming separate basal and apical projections. The branch synapsing in the AVCN is reduced and disorganized. Arrowheads indicate overlapping fibers. The DCN branch is represented by just a few fibers in *Isl1CKO* (*Inset*). (*F* and *G*) Images of individual colors of the separate channels represent projections labeled from the apex (green) and base (red), shown as a merged image in *E*. (*H* and *I*) The confocal section shows segregated cochlear afferents from the base and apex, and vestibular afferents extend toward the control's lateral vestibular nucleus (LVN). In contrast, cochlear afferents of *Isl1CKO* overlap (yellow fibers), and some basal afferents extend toward the CN, and some project toward the LVN and loop back to the CN. (*J*) Graphic summary of aberrant location and projections of auditory neurons in *Isl1CKO*. In the control, the auditory system is tonotopically organized, including neurons of the SG, the AN, and the CN subdivisions. In *Isl1CKO*, excluding some portion of neurons in the base, neurons are located outside of Rosenthal's canal. Some neurons projecting to the cochlea are mixed with vestibular neurons. The central axons are not segregated in the AN and AVCN. Projections entering the DCN are diminished in *Isl1CKO*. AC, anterior crista; D, dorsal; HC, horizontal crista; P, posterior axes; PVCN, posteroventral CN; PC, posterior crista; RB, restiform body; r1-r6, rhombomere 1–6; U, utricle; S, saccule; VN, vestibular nerve. (Scale bars, 100 μm.)

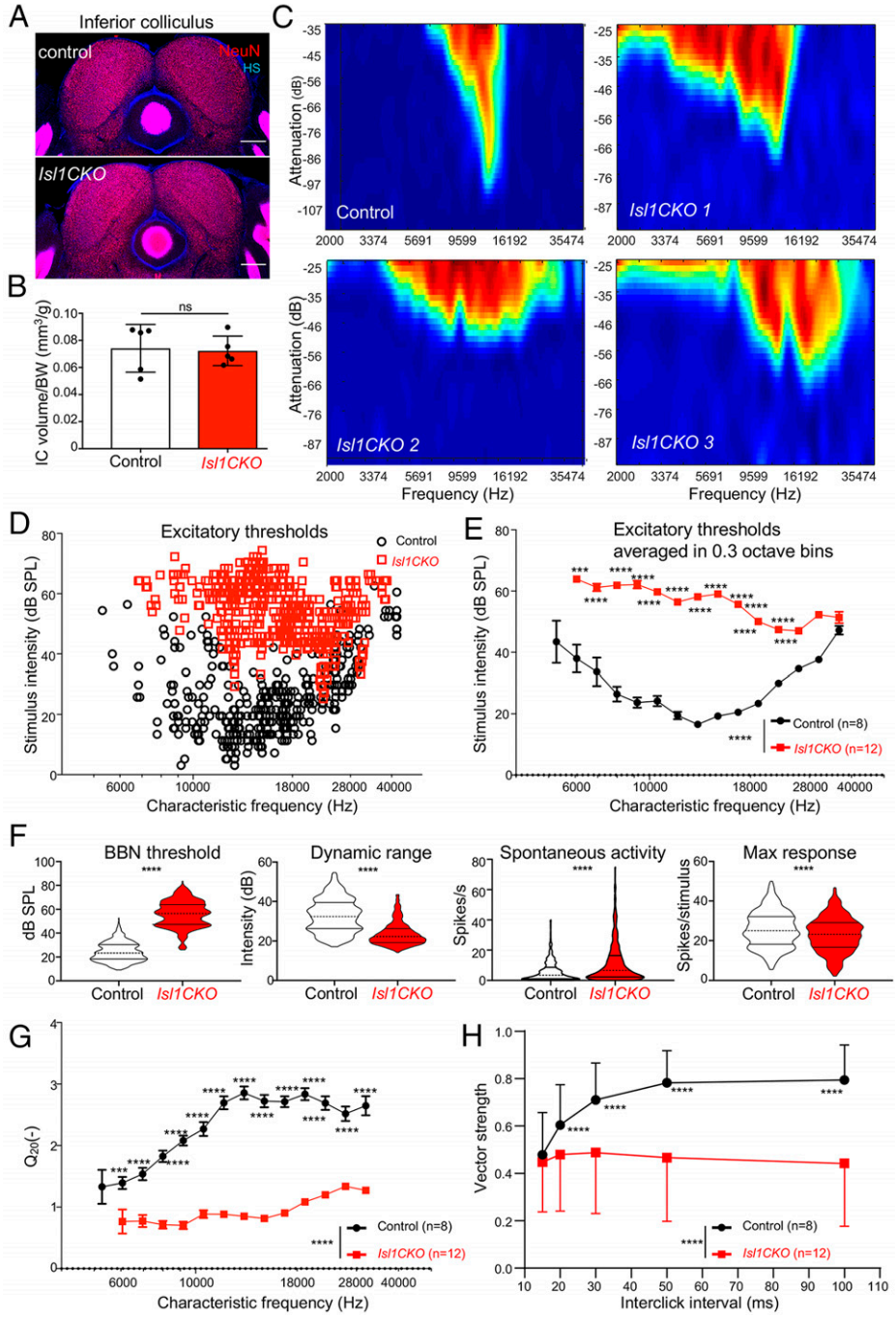

Fig. 6. Characteristics of IC neurons (units) are affected in *Isl1CKO* mice. (*A*) Immunostaining of coronal brain sections for NeuN and nuclear staining Hoechst (HS). (Scale bars, 200 μm.) (*B*) Quantification of the adult control volume and *Isl1CKO* IC adjusted to body weight. Data are expressed as mean ± SD (n = 5 mice per genotype), unpaired t *test* (ns, not significant). (*C*) Representative examples of tuning curves recorded in the IC display impairments in tuning properties with broad and irregular receptive fields in *Isl1CKO* compared to control mice. (*D*) Scatter diagram shows the distribution of the excitatory thresholds of IC neurons in dependency on the CF recorded in control and *Isl1CKO* mice. Note, no IC neurons are recorded below 6 kHz in *Isl1CKO*. (*E*) Excitatory thresholds of the IC neurons at different CFs are shown as averages in 0.3-octave bins in control and *Isl1CKO* mice. Data are expressed as mean ± SEM. Two-way ANOVA with Bonferroni post hoc test. $^{**}P < 0.01$, $^{***}P < 0.001$, $^{****}P < 0.0001$. (*F*) Comparison of the rate intensity function parameters between control (n = 8) and *Isl1CKO* mice (n = 12): BBN threshold, dynamic range, spontaneous activity, and maximum response magnitude. Violin plots indicate median (middle line), 25th, and 75th percentile (dotted lines), unpaired t-test, $^{****}P < 0.0001$. (*G*) The sharpness of the neuronal tuning expressed by quality factor Q_{20} (the ratio between the CF and bandwidth at 20 dB above the minimum threshold) averaged in 0.3-octave bins is decreased in *Isl1CKO*. (*H*) Synchronization of units with click trains. Vector strength computed for different interclick intervals. Data are expressed as mean ± SD, two-way ANOVA with Bonferroni post hoc test, $^{****}P < 0.0001$.

quality factor in *Isl1CKO* (Fig. 6*G*), showing substantially worsened frequency selectivity.

To evaluate the precise temporal representation of sound in the central auditory system, we performed an acoustic stimulation of the IC units with trains of five clicks with different interclick intervals from 100 ms up to 15 ms. In control mice, increasing the time interval between clicks led to a better synchronization of neuronal responses with the individual clicks in the train, implying precision and reliability of temporal sound discrimination ability (Fig. 6*H*). In contrast, the precise temporal decoding in *Isl1CKO* was disrupted, as the synchronization of neuronal responses was significantly lower for the whole range of interclick intervals. The synchronization level of neuronal responses of *Isl1CKO* remains almost constant, suggesting a lack of precise temporal sound processing.

The Auditory Behavior of *Isl1CKO* Mice Is Altered. Next, we evaluated the behavioral responses of *Isl1CKO* to sound stimuli. Since vestibular dysfunctions might influence auditory behavioral responses, we first assessed the vestibular and motor function of *Isl1CKO*. During open-field observations, *Isl1CKO* mice did not display any abnormal locomotor behavior, such as ataxia, difficulty maintaining balance, wagging or vertical bobbing movements of the head, or circling movements. The air-righting test, a basic vestibular function test, and motor function tests on the rotarod demonstrated comparable motor coordination between control and *Isl1CKO* mice (*SI Appendix*, Fig. S9). Concurrently, the size of the sensory epithelia of the vestibular organs and the size of the dorsal root ganglia were unaffected in *Isl1CKO* (*SI Appendix*, Fig. S9). Thus, locomotor activities of *Isl1CKO* were comparable to control mice. The acoustic startle response

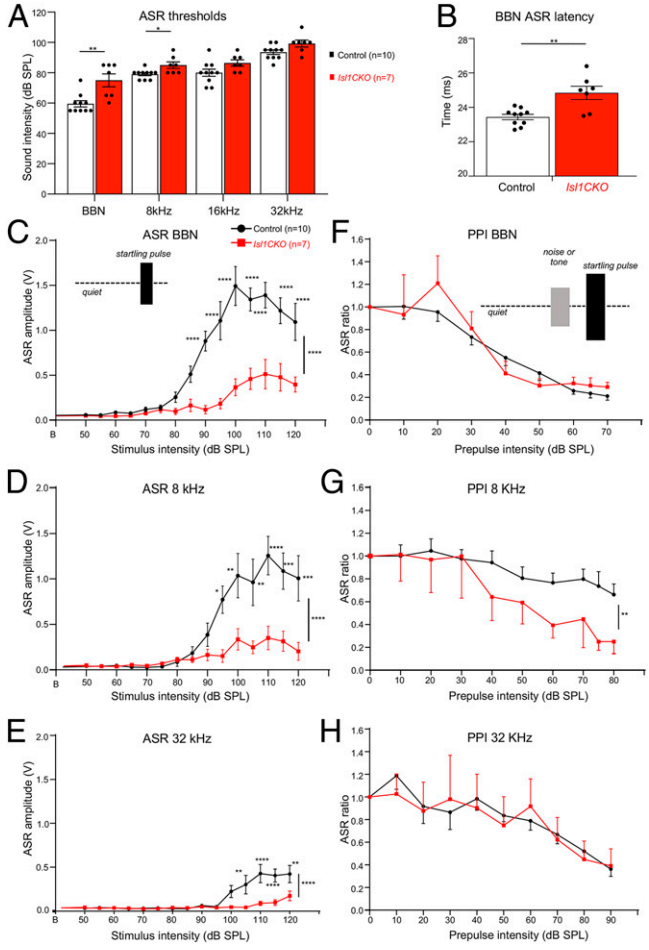

Fig. 7. The ASR and PPI responses are altered in the *Isl1CKO*. (*A*) ASR thresholds for BBN bursts and tone pips at 8, 16, and 32 kHz in control and *Isl1CKO* mice are shown. Holm–Sidak method multiple comparison *t*-test. $*P < 0.05$, $**P < 0.01$. (*B*) Significantly increased ASR latency to BBN is found in *Isl1CKO* compared to control mice; unpaired *t*-test, $**P < 0.01$. (*C*) Amplitude-intensity ASR functions for BBN stimulation and (*D*) for tone pips of 8 kHz and (*E*) 32 kHz at different decibel SPL intensities in control and *Isl1CKO* mice are shown. (*F*) Efficacy of the BBN, (*G*) 8-kHz, and (*H*) 32-kHz tone prepulse intensity on the relative ASR amplitudes are displayed; ASR ratio = 1 corresponds to the ASR amplitude without a prepulse (uninhibited ASR). Two-way ANOVA with Bonferroni post hoc tests. $*P < 0.05$, $**P < 0.01$, $***P < 0.001$, $****P < 0.0001$. All data are expressed as mean ± SEM.

(ASR) is usually used as a behavioral readout of hearing status mediated by a brainstem circuit linking cochlear root neurons to spinal motoneurons. The structural basis of the ASR includes cochlear root neurons, CN neurons, the nucleus of the lateral lemniscus, the caudal pontine reticular nucleus, spinal interneurons, and spinal motor neurons (52, 53). Similar to the ABR thresholds, the ASR thresholds of *Isl1CKO* significantly increased for startle tone stimuli of 8 kHz and BBN, but not for the high-frequency startle tones (Fig. 7*A*). The peak latency of the ASR to the BBN stimulation at the 110-dB sound pressure level (SPL) intensity was prolonged in *Isl1CKO* (Fig. 7*B*), indicating a slower reaction to the acoustic stimuli. We found significantly reduced ASR amplitudes for all tested sound stimuli at higher intensities, showing deteriorated acoustic startle reactivity in *Isl1CKO* mice (Fig. 7 *C*–*E*).

To further assess complex auditory discrimination behavior, we exposed control and *Isl1CKO* mice to a prepulse inhibition (PPI) paradigm (i.e., the inhibition of the ASR induced by presenting an acoustic stimulus shortly preceding the presentation of an acoustic stimulus, the startling sound). The circuit mediating a prepulse on the startle reflex involves central structures of the auditory pathway, including the IC and the auditory cortex (54, 55). We used either BBN or pure-tone pips of 8 and 32 kHz at increasing intensities as a nonstartling acoustic stimulus (prepulse) that preceded the startle stimulus in a quiet background (Fig. 7 *F*–*H*). The PPI with the prepulse of 32 kHz, the well-preserved audible frequency in *Isl1CKO*, was comparable between control and mutant mice. Interestingly, the prepulse of 8 kHz resulted in a more prominent inhibition of the startle response in *Isl1CKO* than in controls, despite the significant hearing deficiency at 8 kHz, as shown by ABR evaluations. This indicates that the 8-kHz prepulse response was enhanced in *Isl1CKO*, suggesting neural hyperactivity of the central auditory system (46, 56). Thus, the ASR and PPI of startle analyses indicate abnormalities in the acoustic behavior of *Isl1CKO*.

Discussion

Our study shows that LIM homeodomain transcription factor ISL1 regulates neuronal development in the cochlea. Using RNA profiling, morphological, and physiological analyses, we provide evidence that ISL1 coordinates genetic networks affecting the molecular characteristics of SGNs, pathfinding abilities, and auditory information processing. The elimination of *Isl1* in neurons during inner ear development results in a migration defect of SGNs, disorganized innervation in the cochlea, unsegregated and reduced central axons, and reduced size of the CN. This neuronal phenotype of *Isl1CKO* was accompanied by hearing impairment, abnormalities in sound processing in the IC, and aberrant auditory behavior. ISL1 is critical for the development of multiple tissues, neuronal and nonneuronal cells (57–61). Different aspects of neuronal development depend on ISL1, including specification of motoneurons (57), sensory neurons (24, 59), axonal growth (62), and axonal pathfinding (63). During inner ear development, ISL1 is expressed in both neuronal and sensory precursors (19, 21, 22). Transgenic modulations of *Isl1* indicate important roles of ISL1 in the maintenance and function of neurons and hair cells and as a possible contributing factor in neurodegeneration (64–67). These studies suggest that ISL1 plays a role in developing neurons and sensory cells, but no direct evaluation of ISL1 function has been performed. To circumvent the pleiotropic effects of *Isl1* in embryonic development, we used *Neurod1*^{Cre} to delete *Isl1* specifically in the inner ear neurons.

We established that ISL1 is necessary for neuronal differentiation programs in the cochlea and the functional properties of the auditory system. Our RNA profiling of SGNs demonstrated transcriptome changes induced by a loss of *Isl1* affecting the molecular characteristics of neurons and pathfinding abilities, including neurotransmission, the structure of synapses, neuron migration, axonogenesis, and expression of crucial guidance molecules. Consistent with the central role of ISL1 in sensory neuron developmental programs (24), regulatory networks of signaling molecules and transcription factors were affected in *Isl1CKO* neurons, such as proneural bHLH factors (members of NeuroD, Olig, and Nscl families), LIM-only (*Lmo2*, *Lmo3*) and LIM homeodomain transcription factors (*Lhx1*, *Lhx2*, *Isl2*), transcription activation complexes for coordination of particular differentiation programs Eyes absent (*Eya4* and *Eya2*) and Sine oculis (*Six2*), POU homeodomain transregulatory factors (*Pou3f2* and *Pou4f2*), and FGF signaling molecules (*Fgf10*, *Fgf11*, *Fgf13*, *Fgf14*) and their downstream targets (*Etv1*, *Etv4*, *Etv5*). Interestingly, the transcription factor *Gata3* was downregulated, suggesting that ISL1 is upstream of the Gata3 transcriptional network of neuronal differentiation programs (14).

Thus, ISL1 orchestrates a complex gene regulatory network driving multiple aspects of neuronal differentiation in the cochlea and defining neuronal features.

The most striking morphological features of the neuronal phenotype of *Isl1CKO* are the aberrant migration and pathfinding of SGNs. A similar migration deficit was reported for *ErbB2*-null mutants (68); however, the interpretation of the findings is convoluted by the compounded direct inner ear effects and the effects associated with neural crest-derived Schwann cells. Additionally, conditional deletion of *Sox10* produced by $Wnt1^{Cre}$ resulted in abnormal migration of SGNs similar to the *Isl1CKO* phenotype (69). Migration defects of SGNs in both *ErbB2* (68) and *Sox10* mutants (69) were attributed to the complete absence of Schwann cells in the entire inner ear ganglion. However, in our *Isl1CKO*, $Sox10^{+}$ Schwann cells were found in a similar density in the spiral ganglion of both mutant and control mice, thus excluding any direct involvement of glial cells in the migration defects of *Isl1*-deficient neurons. We identified several genes with altered molecular profiles that are associated with neuronal phenotypes of projection and migration abnormalities. For example, misplaced SGNs in the modiolus are in *Ntrk2* and *Ntrk3* neurotrophin receptor mutants (36). Less severe phenotypes of misplaced SGNs have been reported for mice lacking *Dcc* (40) or mice with deficient Slit/Robo signaling (39). All these reported SGN migration defects are also associated with abnormalities in projections. In line with the *Isl1CKO* phenotype of deficient neuronal migration and projections, *Isl1* elimination in SGNs resulted in major transcriptional changes of genes encoding members of all four classes of guidance molecules and their receptors, growth factors, neurotrophic factor receptors, and cell adhesion molecules (NCAM family, integrins, cadherins, and protocadherins), among others that are known to participate in molecular networks coordinating neuronal migratory behaviors, axon guidance, and neural circuit assembly.

More profound disorganization of peripheral processes than defects found in *Isl1CKO* or both *ErbB2*-null (68) and *Sox10* mutants (69) was reported for delayed conditional deletion of *Gata3* in SGNs (14). Despite severe disorganization of cochlear wiring of this *Gata3* mutant, central projections maintained their overall tonotopic organization within the auditory nerve and the CN (13, 14). In contrast, we provide compelling evidence that elimination of *Isl1* in SGNs affected the pathfinding abilities of neurons in the cochlea to form peripheral processes and establish central projections. Such profound disorganization of peripheral and central projections is known for *Neurod1* mutations (17, 19, 20). Deletions of *Neurod1* result in miswired and diminished SGNs, and loss of tonotopy (17, 20). Somewhat similar disorganization of central axons with unsegregated auditory nerve fibers, reduced size of the CN, and missing tonotopic organization of synapsing branches in the CN subdivisions was found in our *Isl1CKO*. Although both *Neurod1CKO* and *Isl1CKO* demonstrated significant hearing loss, in contrast to the reduced sound frequency range of *Neurod1CKO* (20), responses for the entire measured frequency range were detected in *Isl1CKO*. The processing of high acoustic frequencies was broadly comparable between age-matched controls and *Isl1CKO*, indicating some preservation of peripheral neuronal activity. Specifically, high frequencies above 28 kHz were comparable between the control and *Isl1CKO* mice, as shown by ABR measurements and extracellular electrophysiological recordings of IC neuronal activity (Figs. 3*B* and 6 *D* and *E*).

As a result of disorganized primary auditory neurons with derailed central projections, the characteristics of persistent auditory function in the IC were altered with worsened tuning capabilities of IC units and their increased spontaneous activity and threshold elevations and decreased dynamic range. The peripheral deficit in sound encoding results in abnormal auditory behavior of *Isl1CKO*. Although no significant differences of ABR thresholds at 32 kHz were observed between *Isl1CKO* and control mice, indicating retained hearing function, the startle reactions of *Isl1CKO* at 32 kHz were reduced. Plasticity of the startle response is also evident in the PPI responses of *Isl1CKO* mice, in which a weak prestimulus suppresses the response to a subsequent startling stimulus. *Isl1CKO* mice demonstrated PPI impairment for the pure tone of 8 kHz, reflecting abnormal sensorimotor gating due to hyperactivity of the central auditory system (56, 70).

Additionally, compared to control mice, DPOAE responses of *Isl1CKO* were reduced, indicating dysfunction of cochlear amplification. The OHCs of the organ of Corti play a central role in the active enhancement of sound-induced vibration. For given OHCs, amplification only occurs at a precise frequency, and thus, this mechanism provides a sharpening of the tuning curve and improves frequency selectivity (71). Nevertheless, DPOAE analysis showed that some function was preserved in high-frequency OHCs in the *Isl1CKO* cochlea. Frequencies above 28 kHz are located at the basal half of the mouse cochlea, from the midbase to the basal end (41), which correspond to the most preserved distribution of sensory neurons in the area of the spiral ganglion of *Isl1CKO* mice. Usually, decreased DPOAE amplitudes indicate loss and dysfunction of OHCs (64, 71–73). Since $Neurod1^{Cre}$ is not expressed in sensory cells in the cochlea, any changes in the development of OHCs represent secondary effects of *Isl1* elimination in neurons. Accordingly, cochlear amplification deficits in *Isl1CKO* correlated with the reduced and disorganized innervation of OHCs (*SI Appendix*, Fig. S4). The medial olivocochlear efferents innervate OHCs from the brainstem, representing a sound-evoked negative feedback loop suppressing OHC activity (74). The formation of efferent intraganglionic spiral bundle was altered in *Isl1CKO*, indicating changes in efferent innervation in the cochlear region. Besides efferents, OHCs are innervated by the type II SGNs (75, 76). Although the function of type II SGNs remains obscure, it is clear that these neurons are involved in auditory nociception (77), and may also constitute the disputed sensory drive for the olivocochlear efferent reflex (78, 79). As *Isl1* is expressed in both type I and type II SGNs during inner ear development (4), characteristics of both neuronal types might likely be affected in *Isl1CKO*. Alternatively, the apical innervation of afferents and efferents could cause a side effect in the *Isl1CKO* mice.

The unexpected close-to-normal hearing function and auditory signal processing at high frequencies suggest some preservation of tonotopic organization in the *Isl1CKO* cochlea for the propagation of acoustic information. Correspondingly, our 3D images of the *Isl1CKO* cochlea show that some neurons in the base are in their proper position in the Rosenthal's canal, forming a segment of the spiral ganglion. These unexpected results may reflect a timeline of sequential neuronal differentiation from the base to the apex, as the first differentiated neurons are in the base and the last SGNs undergo terminal mitosis in the apex (80). As the cochlea extends, differentiating neurons migrate along the cochlea to form the spiral ganglion. This process is completely disrupted in the *Isl1CKO* cochlea, and many neurons are concentrated in a conical-shaped central structure, the modiolus, with only a portion of neurons in the Rosenthal's canal. Notably, the functional and spatial organization of SGNs may differ in transcription factor networks required for their

differentiation programs. For example, some *Neurod1*-lacking neurons survive, form a rudimental cochlear ganglion, and establish bipolar connections to their targets in *Neurod1*-null mice (12) or the otocyst-deleted *Neurod1* conditional mutant (18). Consistent with these findings, neurons forming a segment of the spiral ganglion in the Rosenthal's canal of *Isl1CKO* may not require ISL1 for their differentiation and the migration mode. Another possibility is that *Neurod1*^{Cre} may produce a delayed *Isl1* deletion, resulting in a close-to-normal spatial organization of SGNs and auditory system function at high frequencies. A different Cre driver generating an earlier recombination of *Isl1* in the otocyst might be used to address the high-frequency hearing phenotype of *Isl1CKO*.

Another secondary effect of *Isl1* elimination in neurons likely contributing to the hearing deficit of *Isl1CKO* is a shortened cochlea accompanied by the disorganized apical epithelium. Similar phenotypes of a shortened cochlea were previously reported for deletion mutants of *Neurod1* and *Neurog1*, key transcription factors for inner ear neuronal development (12, 19, 20, 80–82). Although mechanisms affecting the cochlear extension are unknown, it is clear that these confounding features of the *Isl1CKO* phenotype would consequently impact mechanical and neural tuning from the base to the apex of the cochlea and the ability to perform time-frequency processing of sound.

A limitation of our study is that we only assessed the functional role of *Isl1* in the inner ear neurons. Notably, the elimination of *Isl1* in developing neurons is only a part of the story. The expression pattern of ISL1 indicates that ISL1 may control the development of multiple inner ear progenitors (22). The expression of ISL1 in sensory precursors is down-regulated as hair cell differentiation is initiated, and thus ISL1 is not detected in the differentiated sensory hair and supporting cells in vestibular and cochlear epithelia (22). It is conceivable that ISL1 may play a role in the specification of sensory fate and the regulation of the initial sequential events in sensory precursor development. Further studies will be needed to fully uncouple regulatory mechanisms in inner ear development by targeted eliminations of *Isl1* in sensory precursors.

Altogether, our study provides compelling evidence that ISL1 is a critical regulator of SGN development, affecting neuronal migration, pathfinding abilities to form cochlear wiring, and central axonal projections. As such, ISL1 represents an essential factor in the regulation of neuronal differentiation to produce functional neurons in cell-based therapies and stem cell engineering (83, 84). Additionally, this unique model contributes to our understanding of how disorganization of the neuronal periphery affects information processing at higher centers of the central auditory pathway at the physiological and behavioral levels.

Materials and Methods

Experimental Animals. All experiments involving animals were performed according to the NIH *Guide for the Care and Use of Laboratory* Animals (85). The design of experiments was approved by the Animal Care and Use Committee of the Institute of Molecular Genetics, Czech Academy of Sciences (protocol #104/2019). To generate *Isl1CKO* (the genotype *Neurod1*^{Cre};*Isl1*$^{loxP/loxP}$), we cross-bred floxed *Isl1* (*Isl1*$^{loxP/loxP}$; *Isl1*^{tm2Sev}/J, #028501, JAX) (24) and *Neurod1*^{Cre} transgenic mice [Tg(Neurod1-cre)1Able/J, #028364, JAX] (23). Heterozygous animals, *Neurod1*^{Cre};*Isl1*$^{+/loxP}$ were viable, born in appropriate Mendelian ratios, and were phenotypically indistinguishable from control (Cre^{-}) littermate mice. As control mice, we used mice with the genotype Cre^{-}, *Isl1*$^{loxP/loxP}$, and *Isl1*$^{+/loxP}$. We used both males and females for experiments. Phenotyping and data analyses were performed blind to the genotype of the mice. The experimental procedures are detailed in *SI Appendix, Materials and Methods*.

Data, Materials, and Software Availability. All study data are included in the main text and supporting information. The raw RNAseq data were deposited at GEO: (GSE182575) (86).

ACKNOWLEDGMENTS. We thank A. Pavlinek (King's College London) for editing the manuscript and M. Anderova for providing TomatoAi14. This research was supported by the CSF (20-06927S to G.P.); by the Czech Academy of Science RVO 86652036 (to G.P.); and NIH/National Institute on Aging R01 AG060504, DC016099, and AG051443 (to E.N.Y. and B.F.). We acknowledge BIOCEV Imaging Methods Core Facility LM2018129 by MEYS (Ministry of Education, Youth and Sports) and CZ.02.1.01/0.0/0.0/18_046/0016045 by ERDF (European Regional Development Fund); and the Biocev GeneCore Facility and Animal facility (LM 2018126 by MEYS OP RDE CZ.02.1.01/0.0/0.0/18_046/0015861 CCP Infrastructure by MEYS and ESIF (European Structural and Investment Funds)).

Author affiliations: [a]Laboratory of Molecular Pathogenetics, Institute of Biotechnology Czech Academy of Sciences, 25250 Vestec, Czechia; [b]Department of Auditory Neuroscience, Institute of Experimental Medicine Czech Academy of Sciences, 14220 Prague, Czechia; [c]Laboratory of Gene Expression, Institute of Biotechnology Czech Academy of Sciences, 25250 Vestec, Czechia; [d]Laboratory of Light Microscopy, Institute of Molecular Genetics Czech Academy of Sciences, 14220 Prague, Czechia; [e]Department of Physiology, School of Medicine, University of Nevada, Reno, NV 89557; [f]Department of Biology, University of Iowa, Iowa City, IA 52242-1324; and [g]Department of Otolaryngology, University of Iowa, Iowa City, IA 52242-1324

1. M. A. Muniak *et al.*, "Central projections of spiral ganglion neurons" in *The Primary Auditory Neurons of the Mammalian Cochlea*, A. Dabdoub, B. Fritzsch, A. N. Popper, R. R. Fay, Eds. (Springer, New York, NY, 2016) pp. 157–190.
2. E. W. Rubel, B. Fritzsch, Auditory system development: Primary auditory neurons and their targets. *Annu. Rev. Neurosci.* **25**, 51–101 (2002).
3. B. R. Shrestha *et al.*, Sensory neuron diversity in the inner ear is shaped by activity. *Cell* **174**, 1229–1246.e17 (2018).
4. C. Petitpré *et al.*, Neuronal heterogeneity and stereotyped connectivity in the auditory afferent system. *Nat. Commun.* **9**, 3691 (2018).
5. S. Sun *et al.*, Hair cell mechanotransduction regulates spontaneous activity and spiral ganglion subtype specification in the auditory system. *Cell* **174**, 1247–1263.e15 (2018).
6. C. Petitpre *et al.*, Single-cell RNA-sequencing analysis of the developing mouse inner ear identifies molecular logic of auditory neuron diversification. *Nat. Commun.* **13**, 3878 (2022).
7. K. Kandler, A. Clause, J. Noh, Tonotopic reorganization of developing auditory brainstem circuits. *Nat. Neurosci.* **12**, 711–717 (2009).
8. M. Di Bonito, M. Studer, Cellular and molecular underpinnings of neuronal assembly in the central auditory system during mouse development. *Front. Neural Circuits* **11**, 18 (2017).
9. E. A. Lopez-Poveda, Olivocochlear efferents in animals and humans: From anatomy to clinical relevance. *Front. Neurol.* **9**, 197 (2018).
10. B. Fritzsch, K. L. Elliott, Evolution and development of the inner ear efferent system: Transforming a motor neuron population to connect to the most unusual motor protein via ancient nicotinic receptors. *Front. Cell. Neurosci.* **11**, 114 (2017).
11. Q. Ma, D. J. Anderson, B. Fritzsch, Neurogenin 1 null mutant ears develop fewer, morphologically normal hair cells in smaller sensory epithelia devoid of innervation. *J. Assoc. Res. Otolaryngol.* **1**, 129–143 (2000).
12. W.-Y. Kim *et al.*, NeuroD-null mice are deaf due to a severe loss of the inner ear sensory neurons during development. *Development* **128**, 417–426 (2001).
13. J. S. Duncan, B. Fritzsch, Continued expression of GATA3 is necessary for cochlear neurosensory development. *PLoS One* **8**, e62046 (2013).
14. J. M. Appler *et al.*, Gata3 is a critical regulator of cochlear wiring. *J. Neurosci.* **33**, 3679–3691 (2013).
15. E. J. Huang *et al.*, Brn3a is a transcriptional regulator of soma size, target field innervation and axon pathfinding of inner ear sensory neurons. *Development* **128**, 2421–2432 (2001).
16. M. Liu *et al.*, Essential role of BETA2/NeuroD1 in development of the vestibular and auditory systems. *Genes Dev.* **14**, 2839–2854 (2000).
17. I. Jahan, J. Kersigo, N. Pan, B. Fritzsch, Neurod1 regulates survival and formation of connections in mouse ear and brain. *Cell Tissue Res.* **341**, 95–110 (2010).
18. I. Filova *et al.*, Early deletion of *Neurod1* alters neuronal lineage potential and diminishes neurogenesis in the inner ear. *Front. Cell Dev. Biol.* **10**, 845461 (2022).
19. I. Filova *et al.*, Combined *Atoh1* and *Neurod1* deletion reveals autonomous growth of auditory nerve fibers. *Mol. Neurobiol.* **57**, 5307–5323 (2020).
20. I. Macova *et al.*, Neurod1 is essential for the primary tonotopic organization and related auditory information processing in the midbrain. *J. Neurosci.* **39**, 984–1004 (2019).
21. M. Dvorakova *et al.*, Incomplete and delayed Sox2 deletion defines residual ear neurosensory development and maintenance. *Sci. Rep.* **6**, 38253 (2016).
22. K. Radde-Gallwitz *et al.*, Expression of Islet1 marks the sensory and neuronal lineages in the mammalian inner ear. *J. Comp. Neurol.* **477**, 412–421 (2004).
23. H. J. Li, A. Kapoor, M. Giel-Moloney, G. Rindi, A. B. Leiter, Notch signaling differentially regulates the cell fate of early endocrine precursor cells and their maturing descendants in the mouse pancreas and intestine. *Dev. Biol.* **371**, 156–169 (2012).

24. Y. Sun *et al.*, A central role for Islet1 in sensory neuron development linking sensory and spinal gene regulatory programs. *Nat. Neurosci.* **11**, 1283–1293 (2008).
25. I. Jahan, N. Pan, J. Kersigo, B. Fritzsch, Neurod1 suppresses hair cell differentiation in ear ganglia and regulates hair cell subtype development in the cochlea. *PLoS One* **5**, e11661 (2010).
26. C. Li *et al.*, Comprehensive transcriptome analysis of cochlear spiral ganglion neurons at multiple ages. *eLife* **9**, e50491 (2020).
27. E. T. Stoeckli, Understanding axon guidance: Are we nearly there yet? *Development* **145**, dev151415 (2018).
28. B. Fritzsch, J. Kersigo, T. Yang, I. Jahan, N. Pan, "Neurotrophic factor function during ear development: Expression changes define critical phases for neuronal viability" in *The Primary Auditory Neurons of the Mammalian Cochlea*, A. Dabdoub, B. Fritzsch, A. N. Popper, R. R. Fay, Eds. (Springer, New York, NY, 2016) pp. 49–84.
29. D. J. Dennis, S. Han, C. Schuurmans, bHLH transcription factors in neural development, disease, and reprogramming. *Brain Res.* **1705**, 48–65 (2019).
30. T. Yang, J. Kersigo, S. Wu, B. Fritzsch, A. G. Bassuk, Prickle1 regulates neurite outgrowth of apical spiral ganglion neurons but not hair cell polarity in the murine cochlea. *PLoS One* **12**, e0183773 (2017).
31. J. Bok, C. Zenczak, C. H. Hwang, D. K. Wu, Auditory ganglion source of Sonic hedgehog regulates timing of cell cycle exit and differentiation of mammalian cochlear hair cells. *Proc. Natl. Acad. Sci. U.S.A.* **110**, 13869–13874 (2013).
32. S. Pauley *et al.*, Expression and function of FGF10 in mammalian inner ear development. *Dev. Dyn.* **227**, 203–215 (2003).
33. Y. Yu *et al.*, Sensorineural hearing loss and mitochondrial apoptosis of cochlear spiral ganglion neurons in fibroblast growth factor 13 knockout mice. *Front. Cell. Neurosci.* **15**, 658586 (2021).
34. J. Defourny *et al.*, Ephrin-A5/EphA4 signalling controls specific afferent targeting to cochlear hair cells. *Nat. Commun.* **4**, 1438 (2013).
35. T. M. Coate *et al.*, Otic mesenchyme cells regulate spiral ganglion axon fasciculation through a Pou3f4/EphA4 signaling pathway. *Neuron* **73**, 49–63 (2012).
36. B. Fritzsch, M. Barbacid, I. Silos-Santiago, The combined effects of trkB and trkC mutations on the innervation of the inner ear. *Int. J. Dev. Neurosci.* **16**, 493–505 (1998).
37. D. Brors *et al.*, Spiral ganglion outgrowth and hearing development in p75-deficient mice. *Audiol. Neurotol.* **13**, 388–395 (2008).
38. T. M. Coate, N. A. Spita, K. D. Zhang, K. T. Isgrig, M. W. Kelley, Neuropilin-2/Semaphorin-3F-mediated repulsion promotes inner hair cell innervation by spiral ganglion neurons. *eLife* **4**, e07830 (2015).
39. S. Z. Wang *et al.*, Slit/Robo signaling mediates spatial positioning of spiral ganglion neurons during development of cochlear innervation. *J. Neurosci.* **33**, 12242–12254 (2013).
40. Y. J. Kim *et al.*, Dcc mediates functional assembly of peripheral auditory circuits. *Sci. Rep.* **6**, 23799 (2016).
41. M. Müller, K. von Hünerbein, S. Hoidis, J. W. Smolders, A physiological place-frequency map of the cochlea in the CBA/J mouse. *Hear. Res.* **202**, 63–73 (2005).
42. X. Zhou, P. H. Jen, K. L. Seburn, W. N. Frankel, Q. Y. Zheng, Auditory brainstem responses in 10 inbred strains of mice. *Brain Res.* **1091**, 16–26 (2006).
43. T. Chumak *et al.*, BDNF in lower brain parts modifies auditory fiber activity to gain fidelity but increases the risk for generation of central noise after injury. *Mol. Neurobiol.* **53**, 5607–5627 (2016).
44. R. Land, A. Burghard, A. Kral, The contribution of inferior colliculus activity to the auditory brainstem response (ABR) in mice. *Hear. Res.* **341**, 109–118 (2016).
45. S. Wolter *et al.*, GC-B deficient mice with axon bifurcation loss exhibit compromised auditory processing. *Front. Neural Circuits* **12**, 65 (2018).
46. A. R. Chambers *et al.*, Central gain restores auditory processing following near-complete cochlear denervation. *Neuron* **89**, 867–879 (2016).
47. J. A. Harris, E. W. Rubel, Afferent regulation of neuron number in the cochlear nucleus: Cellular and molecular analyses of a critical period. *Hear. Res.* **216–217**, 127–137 (2006).
48. A. M. Lauer, C. J. Connelly, H. Graham, D. K. Ryugo, Morphological characterization of bushy cells and their inputs in the laboratory mouse (*Mus musculus*) anteroventral cochlear nucleus. *PLoS One* **8**, e73308 (2013).
49. K. Karmakar *et al.*, Hox2 genes are required for tonotopic map precision and sound discrimination in the mouse auditory brainstem. *Cell Rep.* **18**, 185–197 (2017).
50. T. Fujiyama *et al.*, Inhibitory and excitatory subtypes of cochlear nucleus neurons are defined by distinct bHLH transcription factors, Ptf1a and Atoh1. *Development* **136**, 2049–2058 (2009).
51. K. G. Gruters, J. M. Groh, Sounds and beyond: Multisensory and other non-auditory signals in the inferior colliculus. *Front. Neural Circuits* **6**, 96 (2012).
52. J. S. Yeomans, P. W. Frankland, The acoustic startle reflex: Neurons and connections. *Brain Res. Brain Res. Rev.* **21**, 301–314 (1995).
53. M. Koch, The neurobiology of startle. *Prog. Neurobiol.* **59**, 107–128 (1999).
54. N. R. Swerdlow, M. A. Geyer, D. L. Braff, Neural circuit regulation of prepulse inhibition of startle in the rat: Current knowledge and future challenges. *Psychopharmacology (Berl.)* **156**, 194–215 (2001).
55. R. H. Fitch, S. W. Threlkeld, M. M. McClure, A. M. Peiffer, Use of a modified prepulse inhibition paradigm to assess complex auditory discrimination in rodents. *Brain Res. Bull.* **76**, 1–7 (2008).
56. A. E. Hickox, M. C. Liberman, Is noise-induced cochlear neuropathy key to the generation of hyperacusis or tinnitus? *J. Neurophysiol.* **111**, 552–564 (2014).
57. S. L. Pfaff, M. Mendelsohn, C. L. Stewart, T. Edlund, T. M. Jessell, Requirement for LIM homeobox gene Isl1 in motor neuron generation reveals a motor neuron-dependent step in interneuron differentiation. *Cell* **84**, 309–320 (1996).
58. L. Yang *et al.*, Isl1Cre reveals a common Bmp pathway in heart and limb development. *Development* **133**, 1575–1585 (2006).
59. K. Huber *et al.*, The LIM-Homeodomain transcription factor Islet-1 is required for the development of sympathetic neurons and adrenal chromaffin cells. *Dev. Biol.* **380**, 286–298 (2013).
60. U. Ahlgren, S. L. Pfaff, T. M. Jessell, T. Edlund, H. Edlund, Independent requirement for ISL1 in formation of pancreatic mesenchyme and islet cells. *Nature* **385**, 257–260 (1997).
61. C. L. Cai *et al.*, Isl1 identifies a cardiac progenitor population that proliferates prior to differentiation and contributes a majority of cells to the heart. *Dev. Cell* **5**, 877–889 (2003).
62. X. Liang *et al.*, Isl1 is required for multiple aspects of motor neuron development. *Mol. Cell. Neurosci.* **47**, 215–222 (2011).
63. A. Kania, T. M. Jessell, Topographic motor projections in the limb imposed by LIM homeodomain protein regulation of ephrin-A:EphA interactions. *Neuron* **38**, 581–596 (2003).
64. T. Chumak *et al.*, Deterioration of the medial olivocochlear efferent system accelerates age-related hearing loss in Pax2-Isl1 transgenic mice. *Mol. Neurobiol.* **53**, 2368–2383 (2016).
65. R. Bohuslavova *et al.*, Pax2-Islet1 transgenic mice are hyperactive and have altered cerebellar foliation. *Mol. Neurobiol.* **54**, 1352–1368 (2017).
66. M. Huang, A. Kantardzhieva, D. Scheffer, M. C. Liberman, Z. Y. Chen, Hair cell overexpression of Islet1 reduces age-related and noise-induced hearing loss. *J. Neurosci.* **33**, 15086–15094 (2013).
67. T. Chumak *et al.*, Overexpression of *Isl1* under the *Pax2* promoter, leads to impaired sound processing and increased inhibition in the inferior colliculus. *Int. J. Mol. Sci.* **22**, 4507 (2021).
68. J. K. Morris *et al.*, A disorganized innervation of the inner ear persists in the absence of ErbB2. *Brain Res.* **1091**, 186–199 (2006).
69. Y. Mao, S. Reiprich, M. Wegner, B. Fritzsch, Targeted deletion of Sox10 by Wnt1-cre defects neuronal migration and projection in the mouse inner ear. *PLoS One* **9**, e94580 (2014).
70. M. A. Geyer, K. L. McIlwain, R. Paylor, Mouse genetic models for prepulse inhibition: An early review. *Mol. Psychiatry* **7**, 1039–1053 (2002).
71. M. LeMasurier, P. G. Gillespie, Hair-cell mechanotransduction and cochlear amplification. *Neuron* **48**, 403–415 (2005).
72. P. Dallos *et al.*, Prestin-based outer hair cell motility is necessary for mammalian cochlear amplification. *Neuron* **58**, 333–339 (2008).
73. A. Herranen *et al.*, Deficiency of the ER-stress-regulator MANF triggers progressive outer hair cell death and hearing loss. *Cell Death Dis.* **11**, 100 (2020).
74. L. D. Liberman, M. C. Liberman, Cochlear efferent innervation is sparse in humans and decreases with age. *J. Neurosci.* **39**, 9560–9569 (2019).
75. A. Hafidi, Peripherin-like immunoreactivity in type II spiral ganglion cell body and projections. *Brain Res.* **805**, 181–190 (1998).
76. K. L. Elliott *et al.*, Developmental changes in *Peripherin*-eGFP expression in spiral ganglion neurons. *Front. Cell. Neurosci.* **15**, 678113 (2021).
77. K. D. Zhang, T. M. Coate, Recent advances in the development and function of type II spiral ganglion neurons in the mammalian inner ear. *Semin. Cell Dev. Biol.* **65**, 80–87 (2017).
78. K. E. Froud *et al.*, Type II spiral ganglion afferent neurons drive medial olivocochlear reflex suppression of the cochlear amplifier. *Nat. Commun.* **6**, 7115 (2015).
79. S. Maison, L. D. Liberman, M. C. Liberman, Type II cochlear ganglion neurons do not drive the olivocochlear reflex: Re-examination of the cochlear phenotype in peripherin knock-out mice. *eNeuro* **3**, ENEURO.0207-16.2016 (2016).
80. V. Matei *et al.*, Smaller inner ear sensory epithelia in Neurog 1 null mice are related to earlier hair cell cycle exit. *Dev. Dyn.* **234**, 633–650 (2005).
81. S. Pauley, E. Lai, B. Fritzsch, Foxg1 is required for morphogenesis and histogenesis of the mammalian inner ear. *Dev. Dyn.* **235**, 2470–2482 (2006).
82. D. H. Nichols *et al.*, Lmx1a is required for segregation of sensory epithelia and normal ear histogenesis and morphogenesis. *Cell Tissue Res.* **334**, 339–358 (2008).
83. G. Pavlinkova, Molecular aspects of the development and function of auditory neurons. *Int. J. Mol. Sci.* **22**, 131 (2020).
84. A. Zine, Y. Messat, B. Fritzsch, A human induced pluripotent stem cell-based modular platform to challenge sensorineural hearing loss. *Stem Cells* **39**, 697–706 (2021).
85. National Research Council, *Guide for the Care and Use of Laboratory Animals* (National Academies Press, Washington, DC, 1996).
86. I. Filova *et al.*, ISL1 is necessary for auditory neuron development and contributes toward tonotopic organization. NCBI Gene Expression Omnibus. https://www.ncbi.nlm.nih.gov/geo/query/acc.cgi?acc=GSE182575. Deposited 23 August 2021.